HHS Public Access

Author manuscript

J Glaucoma. Author manuscript; available in PMC 2022 May 01.

Published in final edited form as:

J Glaucoma. 2021 May 01; 30(5): e222–e226. doi:10.1097/IJG.0000000000001809.

Semi-Automated Assessment of Anterior Segment Structures in Pediatric Glaucoma using Quantitative Ultrasound Biomicroscopy

Janet Leath Alexander, MD[1], **Snehaa Maripudi, MD**[1], **Karun Kannan, BS**[2], **Jennifer Drechsler, BS**[1], **Moran R. Levin, MD**[1], **Osamah J. Saeedi, MD**[1], **Mona Kaleem, MD**[3], **Marlet Bazemore, MD**[4], **Bethany Karwoski, MD**[4], **Camilo Martinez, COT**[4], **Mohamad Jaafar, MD**[4], **William Patrick Madigan, MD**[4]

[1]Department of Ophthalmology and Visual Sciences, University of Maryland School of Medicine, 419 West Redwood Street, Suite 479, Baltimore, MD 21201

[2]Johns Hopkins University, Department of Computer Science and Engineering, 3400 N. Charles St., Baltimore, MD 21218, USA

[3]Wilmer Eye Institute, Johns Hopkins University, 3400 N. Charles St., Baltimore, MD 21218, USA

[4]Department of Ophthalmology, Children's National Health System, 111 Michigan Avenue, Washington, DC 20010, USA

Abstract

The study was a prospective observational study comparing semi-automated to manual quantitative ultrasound biomicroscopy image analysis among 82 images from 41 eyes of 32 subjects (21 controls and 11 glaucoma) enrolled in the Pediatric Anterior Segment Imaging Innovation Study. Interclass correlation coefficients and correlation coefficients were greater than 0.8 for all parameters, and comparison of respective analysis speed was 7 times faster for the semi-automated method compared to manual image quantification.

Keywords

Ultrasound biomicroscopy; high frequency ultrasound; Image analysis; Cornea; Anterior segment; Pediatric; Congenital glaucoma

Introduction

Primary and secondary causes of early childhood glaucoma can cause physical changes to individual structures of the anterior and posterior segment. Glaucomatous structural changes can be clinically subtle or dramatic, depending on the severity, and include increased corneal diameter and thickness, horizontal striations, and increased axial length. Structural changes are thought to be due to the unique state of collagen in the pediatric eye featuring decreased

Corresponding Author: Janet Leath Alexander, MD, 419 West Redwood Street, Suite 479, Baltimore, MD 21201, USA, Telephone: 667-214-1330, Fax: 410-328-6503, jalexander@som.umaryland.edu.

stromal collagen fibril cross-linking, increased hydration, and increased collagen fiber crimp structure. The specialized collagen architecture of youth results in more elastic biomechanical corneal properties, and allows for enlargement and distortion of the collagenous corneal and scleral stroma.[1–5] The ability to precisely quantify and monitor corneal and axial change is the mainstay of congenital glaucoma monitoring, in addition to frequent measurement of IOP.

Ultrasound biomicroscopy (UBM) allows for a high-resolution view of the anterior segment and offers a unique opportunity for visualization of the anatomy impacted by pediatric glaucoma. Due to high frequency sound waves in the range of 40–50 MHz, UBM offers a span of depth of approximately 5 millimeters, and thus can be used to image the cornea, lens, iris, and ciliary body. UBM has demonstrated several clinically useful characterizations for structures involved in pediatric glaucoma[6] and, unlike all other available imaging modalities, UBM is not hindered by clouding of the cornea. Anterior segment optical coherence tomography (AS-OCT) has similar clinical utility to UBM, with better resolution, but is inferior to UBM in the setting of corneal clouding or for imaging structures posterior to the iris. Established standardized UBM image measurement protocols with manual image analysis using ImageJ have previously demonstrated good intra-observer repeatability and inter-observer agreement.[7]

Some of the major drawbacks to use of UBM in a clinical setting are lack of standardized normative values, time-intensive image analysis, and the requirement for high level knowledge and extensive training. Due to these challenges, UBM use is typically limited to cases where the corneal view is profoundly compromised, or when clinical concern relates to structures posterior to the iris. While these applications are worthy of a dedicated imaging tool, the potential use of the UBM is much greater than these few niche applications. A rapid quantitative assessment tool may allow clinicians additional objective data that may influence diagnosis or management. The development of rapid quantitative analysis for UBM images introduces the emerging field of Quantitative UBM or Q-UBM.

The purpose of our study was to develop a novel open access Q-UBM image analysis tool and evaluate its use in subjects with and without history of congenital glaucoma. Our research team utilized Python open source programming language for semi-automated analysis of UBM images. This program, EyeMark, is able to measure anterior segment structures, including those that may be altered in patients with glaucoma, improving the utility of UBM in a clinical setting and addressing the problems of manual UBM image interpretation.

Materials and Methods

UBM images were obtained from 41 eyes of 32 subjects (21 healthy age-matched subjects and 11 subjects with history of infantile glaucoma) enrolled in the Pediatric Anterior Segment Imaging Innovation Study (PASIIS) (Baltimore, MD). PASIIS is a collaborative program between the University of Maryland and Children’s National Medical Center designed to apply advances in technology and image analysis specifically to clinical

evaluation and management of pediatric anterior segment disease. Demographics are displayed in the Table 1.

Participants were enrolled at the time of ocular examination. Consent for participation in the UBM imaging and analysis was obtained from the parent(s) or participant. Inclusion criteria for infantile glaucoma participants required onset of glaucoma prior to age 2 years. Glaucoma was defined as IOP greater than 21 mmHg, with one or more of the following: corneal enlargement, progressive myopic shift coupled with increasing corneal diameter and/or axial length, increased optic nerve cup-to-disc ratio greater than or equal to 0.2, or a surgical procedure for IOP control.[11] Exclusion criteria for control participants included eyes with abnormal visual function for age, history of traumatic injury, past or present glaucoma or glaucoma suspect status, abnormal gonioscopy, refractive error greater than 4 diopters of hyperopia or myopia, or more than 2 diopters of astigmatism.

This study adhered to the ethical principles outlined in the Declaration of Helsinki as amended in 2013. The Institutional Review Board has approved the above referenced protocol and the associated consent forms. Collection and evaluation of protected health information was compliant with the Health Insurance Portability and Accountability Act of 1996.

A total of 82 UBM images (2 from each eye) were obtained using the Aviso Ultrasound Platform A/B UBM with 50 MHz linear transducer (Quantel Medical, Clermont-Ferrand, France) or the Accutome UBM Plus Platform with 48 MHz linear transducer (Keeler Accutome, Inc. Malvern, PA). Studies have shown no significant difference in measurements of anterior segment structures in children and adults between different anterior segment imaging platforms, including UBM.[8–11] The PASIIS standardized protocol was developed to extract quantitative data from both UBM and AS-OCT images. Imaging techniques have been previously described.[12] Good repeatability and reliability of landmark identification in axial UBM images for structural measurements has been previously established.[7] Our imaging protocol included two UBM images, one horizontal axial and one vertical axial image per eye, in focus at the pupil center. Images were selected based on overall image quality, centration of the pupil, symmetry of the two angles, with resolution sufficient to localize the scleral spur on each side of the image, and identification of landmarks including the corneal center and angles. All images were de-identified and measured by a masked observer.

Parameters measured included angle-to-angle distance (AA), central corneal thickness (CCT), anterior corneal radius of curvature (ACRC), posterior corneal radius of curvature (PCRC), and anterior chamber depth (ACD). Images were measured in two ways: manual measurements using ImageJ and semi-automated measurements using Python EyeMark. ImageJ 1.52a (National Institute of Health, Bethesda, MD, USA), is a Java-based open access image processing program.[13] The ImageJ measurements were performed according to the PASIIS protocol.[7,12] Reliability and repeatability analysis of the ImageJ analysis protocol has been previously published.[7] The semi-automated UBM image analysis protocol was developed using Python 3.7.4 (Python Software Foundation, Fredericksburg, VA, USA).[14] EyeMark relies on the user to select 8 points (two points on the caliper reference line, two

angle apices, central corneal endothelium, central corneal epithelium, and two points on the peripheral corneal epithelium), to calculate the various metrics of the eye as seen in Figure 1. Using these 8 points, EyeMark is able to calculate angle to angle distance (AA), central corneal thickness (CCT), anterior corneal radius of curvature (ACRC), posterior corneal radius of curvature (PCRC), and anterior chamber depth (ACD). [Figure 1][Table 1]

Statistical analysis was performed with Microsoft Excel (2019 Edition; Microsoft). Means for each parameter were determined (Table 1). Corresponding values were compared using analysis of variance (ANOVA) and the interclass correlation coefficient (ICC) was calculated across each set of 82 data points, with an ICC of greater than 0.8 indicating very good reliability and an ICC of greater than 0.9 indicating excellent reliability. Conditional correlation was determined by computing the correlation coefficient (R value) for each parameter along with the p-value. An R value greater than 0.8 was accepted to indicate a strong positive correlation. Bland-Altman plots were constructed to evaluate agreement between manual (ImageJ) and semi-automated (Python EyeMark) methods.

The time to measure each image with ImageJ was recorded for each of ten images. The EyeMark program was run three times for all 82 images and the overall time was divided by the number of images to determine the average amount of time required to measure one image with EyeMark.

Results

Intraclass correlation coefficients (ICC) and correlation coefficients (R values) for each parameter are shown in Table 2. Bland Altman plots and correlation curves are shown in Figure 2A. When participants are separated by glaucoma status, the correlation between ImageJ and EyeMark remains unchanged across all parameters regardless of whether the participant has a diagnosis of congenital glaucoma (Figure 2B). The R value for participants with glaucoma is 0.99 ($p<0.001$) and the R value for participants without glaucoma is similar at 0.99 ($p<0.001$). The average evaluation time per image using ImageJ is 6 min 57 seconds with a standard deviation of 2 minutes and 38 seconds. The average evaluation time per image using EyeMark is 54 seconds per image. [Table 2][Figure 2]

Discussion

The purpose of this project was to determine if the clinical utility of UBM can be improved by semi-automation. A useful image analysis process must yield results that are: 1) Consistent with known values; 2) Repeatable and reliable compared to gold standard; 3) Applicable in both disease and non-disease states; and 4) Faster than current standard image analysis. Based upon our results, the EyeMark automated analysis tool fit each of these criteria when compared to ImageJ manual analysis. Previous studies established cross-platform reproducibility, longitudinal reproducibility, and inter-operator reproducibility,[7–11] while the current study focused exclusively on the comparison of semi-automated and manual techniques. Semi-automation represents a key translational step in advancing the clinical relevance of Q-UBM imaging, to expand on the use of UBM for predominantly qualitative purposes.

ImageJ and EyeMark both extracted data consistent with expected values (Table 1), and well-established patterns were observed when comparing between the glaucoma and control groups. Greater cross-sectional chamber distance (AA), thicker CCT, flatter curvature (ACRC and PCRC), and deeper chamber (ACD) were measured among participants with congenital glaucoma. In comparing the repeatability and reliability of semi-automated compared to manual image analysis, the ICC for all parameters was 0.81 or greater, indicating good reliability with the use of EyeMark. The ICC for AA and PCRC in particular showed excellent reliability. The R values for all parameters was 0.86 or greater, implying strong correlation between measurements taken by ImageJ and EyeMark. Bland Altman plots suggested no systematic proportional bias. The difference between methods did not systematically tend to grow larger or smaller as the mean increases. Variability was consistent without increase in scatter as the mean increases (or decreases), with an exception in CCT for values greater than 800 microns. This feature of the measurement highlights the importance of using the same measurement tool consistently for longitudinal assessment of corneal thickness. Data among glaucoma and non-glaucoma age-matched control eyes show similar correlation, demonstrating that our semi-automated Q-UBM EyeMark program produced accurate measurements regardless of glaucoma status (Figure 2). Lastly, the time-to-analyze was 7-fold less in the automated analysis, confirming the efficiency advantage of semi-automation.

A relatively small sample size was evaluated in this study. While appropriate to answer the question of reliability in this specific use case, absolute values may not apply at the population level. Subjects included eyes with and without history of congenital glaucoma according to well-defined diagnostic criteria, and a broad range of patient ages for both glaucoma and control subjects. Results may generalize to images of similar quality and features, but may not generalize to image analysis involving more profound anterior segment pathology or disorganization, or lower image quality. Measurement of parameters with more complex geometry than the five parameters in this study may likewise have lower repeatability and reliability. The accuracy and precision of EyeMark is dependent on proper identification of anatomical features on ultrasound images. The Python EyeMark program makes assumptions about the geometry of the eye. The epithelium and endothelium of the cornea are assumed to fit into the curvature of a circle, a well-established assumption which governs the use of diopters to describe the cornea. Some disease processes violate this assumption, including trauma and keratoconus. More complex geometric patterns must be taken into account when applying this tool to various disease categories. Unique ocular pathology should be considered at the time of user input. The time-to-evaluate analysis does not take into account training time of the analyst prior to use. We do not intend to disregard that early steps in image analysis training are relevant and sometimes challenging hurdles to overcome.

Python EyeMark semi-automated UBM image analysis provides a more time efficient quantitative UBM analysis without sacrificing data accuracy when compared to ImageJ manual image analysis among subjects with and without history of congenital glaucoma. The clinical implications of using EyeMark for UBM of the anterior segment are broad. Longitudinal studies will be essential to fully understand the utility of this program in clinical context. As with all novel ophthalmic imaging tools and programs, potential

applications are discovered and optimized through use. Please visit github.com/karunkannan/EyeMark to access the program.

Acknowledgments

Support:

The authors have no conflicts of interest to disclose. Dr. Saeedi has received research grants from Vasoptic, Inc and research support from Heidelberg Engineering and declares no relevant conflict of interest. Dr. Maripudi and Ms. Drechsler received funding support from the Proposed Research Initiated by Students and Mentors (PRISM) Program, University of Maryland, Baltimore, MD (UMB). Dr. Alexander has received research grants in collaboration with Vasoptic, Inc and declares no relevant conflict of interest. Dr. Alexander received funding support from the Knights Templar Eye Foundation Career Starter Grant, and the UBM ICTR/Clinical Science and Translational Science KL2 Award 1KL2TR003099-01. We acknowledge the support of the University of Maryland (UM), Baltimore, Institute for Clinical and Translational Research (CTR), UM Center for Innovative Biomedical Resources, UM Medicine Biorepository and the National Center for Advancing Translational Sciences (NCATS) Clinical Translational Science Award (CTSA) grant number 1UL1TR003098.

References

1. Grytz R, Fazio MA, Libertiaux V, et al. Age- and race-related difference in human scleral material properties. Invest Ophthalmol Vis Sci. 2014;55:8163–8172. [PubMed: 25389203]
2. Liu B, McNally S, Kilpatrick JI, Jarvis SP, O'Brien CJ. Aging and ocular tissue stiffness in glaucoma. Surv Ophthalmol. 2018; 63:56–74. [PubMed: 28666629]
3. Studer H, Larrea X, Riedwyl H, Buchler P. Biomechanical model of human cornea based on stromal microstructure. J Biomech. 2010;43:836–842. [PubMed: 20006338]
4. Elsheikh A, Wang D, Brown M, Rama P, Campanelli M, Pye D. Assessment of corneal biomechanical properties and their variation with age. Curr Eye Res. 2007;32:11–19. [PubMed: 17364730]
5. Gogola A, Jan NJ, Brazile B, Lam P, Lathrop KL, Chan KC, Sigal IA. Spatial Patterns and Age-Related Changes of the Collagen Crimp in the Human Cornea and Sclera. Invest Ophthalmol Vis Sci. 2018 6 1;59(7):2987–2998. [PubMed: 30025116]
6. Alexander JL, Wei L, Palmer J, Darras A, Levin MR, Berry JL, Ludeman E. A systematic review of ultrasound biomicroscopy use in pediatric ophthalmology. Eye (Lond). 2020 9 22. doi: 10.1038/s41433-020-01184-4. Epub ahead of print. PMID: 32963311.
7. Qureshi A, Chen H, Saeedi O, Kaleem MA, Stoleru G, Margo J, Kalarn S, Alexander JL. Anterior segment ultrasound biomicroscopy image analysis using ImageJ software: Intra-observer repeatability and inter-observer agreement. Int Ophthalmol. 2019 4;39(4):829–837. [PubMed: 29516316]
8. Chan B, Cho P, Cheung SW. Repeatability and agreement of two A-scan ultrasonic biometers and IOLMaster in non-orthokeratology subjects and post-orthokeratology children. Clin Exp Optom. 2006;89(3):160–168. doi:10.1111/j.1444-0938.2006.00029. [PubMed: 16637971]
9. Radhakrishnan S, Goldsmith J, Huang D, et al. Comparison of optical coherence tomography and ultrasound biomicroscopy for detection of narrow anterior chamber angles. Arch Ophthalmol. 2005;123(8):1053–1059. doi:10.1001/archopht.123.8.1053. [PubMed: 16087837]
10. Mansouri K, Sommerhalder J, Shaarawy T. Prospective comparison of ultrasound biomicroscopy and anterior segment optical coherence tomography for evaluation of anterior chamber dimensions in European eyes with primary angle closure. Eye (Lond). 2010;24(2):233–239. doi:10.1038/eye.2009.103. [PubMed: 19444291]
11. Mansoori T, Balakrishna N. Anterior segment morphology in primary angle closure glaucoma using ultrasound biomicroscopy. J Curr Glaucoma Pract. 2017;11(3):86–91. doi:10.5005/jp-journals-10028-1230 [PubMed: 29151682]
12. Maripudi S, Byrd J, Qureshi A, Stoleru G, Levin MR, Saeedi OJ, Munir W, Bazemore M, Karwoski B, Martinez C, Jaafar MS, Madigan WP, Alexander JL. Pediatric Corneal Structural Development During Childhood Characterized by Ultrasound Biomicroscopy. J Pediatr

Ophthalmol Strabismus. 2020 7 1;57(4):238–245. doi: 10.3928/01913913-20200506-01. PMID: 32687208. [PubMed: 32687208]

13. Schneider CA, Rasband WS, Eliceiri KW “NIH Image to ImageJ: 25 years of image analysis”. Nature Methods 9, 671–675, 2012. Available at: https://imagej.net/ImageJ. [PubMed: 22930834]
14. van Rossum G, Python tutorial, Technical Report CS-R9526, Centrum voorWiskunde en Informatica (CWI), Amsterdam, 5 1995. Python Software Foundation. Python Language Reference. Available at: http://www.python.org.

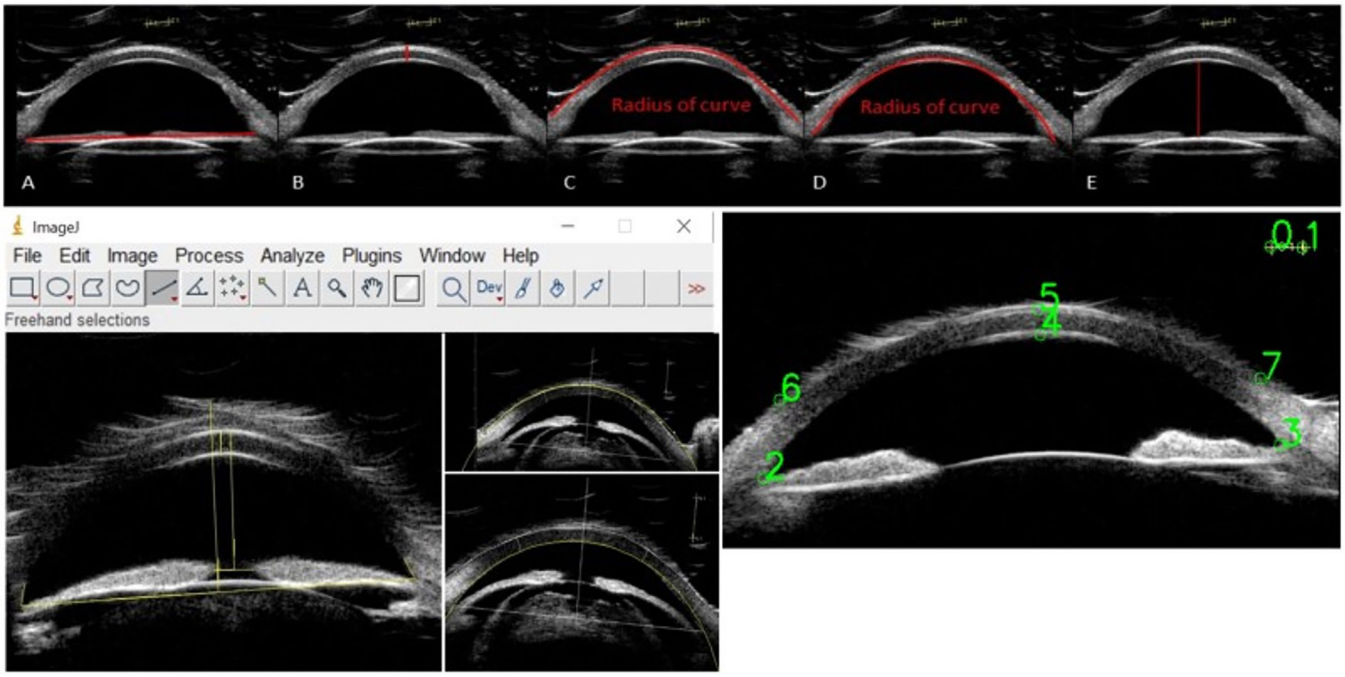

Figure 1:

A-E) Sample measurements of AA, CCT, ACRC, PCRC, ACD, respectively; F) Manual ImageJ user interface with sample measurements; G) Automated EyeMark user interface with sample user input.

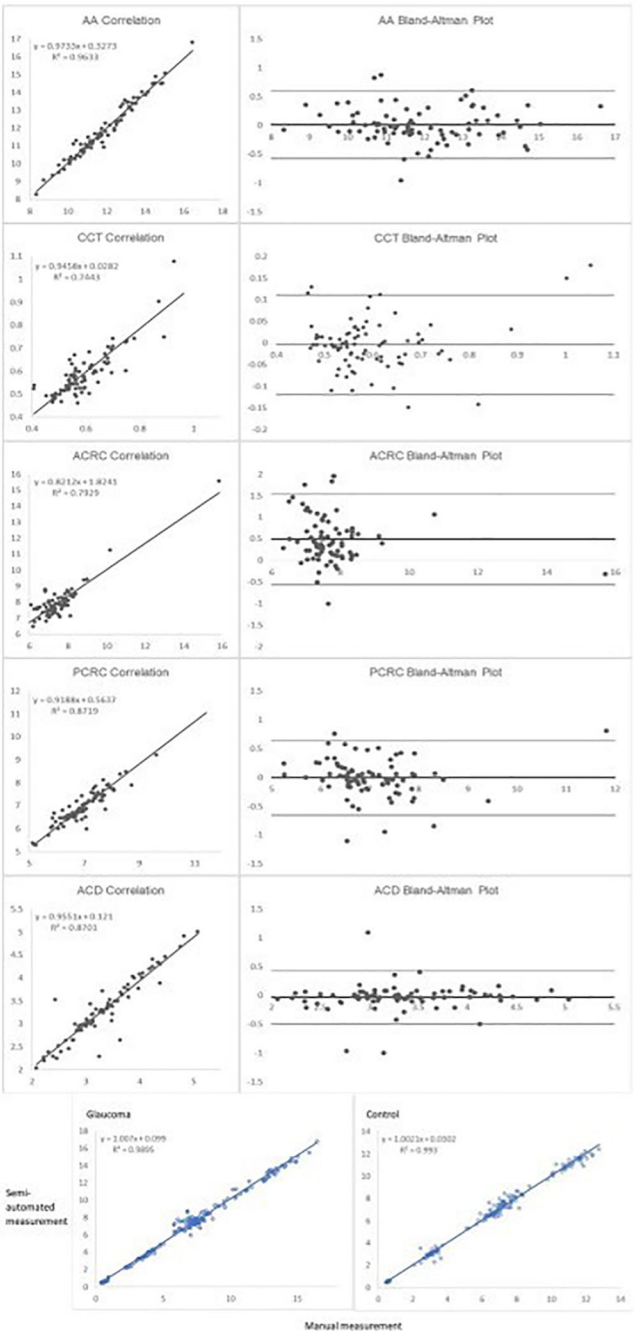

Figure 2:

A. Correlation and Bland-Altman plots for each parameter. B. Correlation among all parameters for semi-automated (EyeMark) vs manual (ImageJ) among subjects with glaucoma (left) and control subjects (right).

Table 1:

Demographics and measurement results in glaucoma and control groups

	Glaucoma		Controls	
Number of Subjects	11 (20 eyes)		21 (21 eyes)	
Gender (% Female)	52%		36%	
Mean Age (months)	9 ± 14		9±12	
Median Age (months)	3		4	
Age range (months)	0–564		0–600	
Race/ethnicity (%)				
African American	73%		52%	
Caucasian	27%		29%	
Hispanic	0%		14%	
Multiple	0%		5%	
	Manual	**Automated**	**Manual**	**Automated**
AA (mm)	12.7 ± 1.7	12.7 ± 1.7	11.1 ± 0.83	11.1 ± 0.91
CCT (mm)	0.642 ± 0.141	0.634 ± 0.130	0.544 ± 0.049	0.561 ± 0.054
ACRC (radius)[diopters]	8.23 [41.00] ± 1.43	7.56 [44.75] ± 1.61	7.72 [43.75] ± 0.50	7.41 [45.50] ± 0.51
PCRC (radius)[diopters]	7.42 [45.50] ± 1.03	7.42 [45.50] ± 1.03	6.59 [51.25] ± 0.48	6.60 [51.25] ± 0.55
ACD (mm)	3.59 ± 0.76	3.62 ± 0.75	3.06 ± 0.37	3.09 ± 0.33

Table 2:

Intraclass correlation coefficients (ICC) and correlation coefficient (R) for automated compared to manual image analysis for 5 parameters.

Parameter	ICC	R	P-value
AA	0.98	0.98	<0.001
CCT	0.86	0.86	<0.001
ACRC	0.81	0.89	<0.001
PCRC	0.93	0.93	<0.001
ACD	0.93	0.93	<0.001